Int J CARS (2015) 10:447–458
DOI 10.1007/s11548-014-1104-y

ORIGINAL ARTICLE

Real-time aortic valve segmentation from transesophageal echocardiography sequence

Junfeng Cai · Xiahai Zhuang · Yuanyuan Nie · Zhe Luo · Lixu Gu

Received: 29 April 2014 / Accepted: 15 July 2014 / Published online: 3 August 2014

Abstract
Purpose Geometric features of the aortic valve play an important role in many applications, such as the clinical diagnostics, shape modeling and image-guided cardiac interventions, especially for the transcatheter aortic valve implantation (TAVI) procedure. However, few works have been reported on the topic of aortic valve segmentation from transesophageal echocardiography (TEE) sequences. To obtain accurate segmentation results and further provide valid support for TAVI, this paper presents a real-time method for segmenting the aortic valve from intraoperative, short-axis view TEE sequences, using an improved probability estimation and continuous max-flow (CMF) approach.
Methods The proposed segmentation method includes two key stages: (1) In the probability estimation stage, five different prior frames spanning a cardiac circle are firstly selected with the aortic valve manually segmented by an expert. Then, the improved composite probability estimation (CPE) and single probability estimation (SPE) over the five prior frames are, respectively, constructed based on their radial average intensity and radial distance. (2) In the energy function construction stage, the similarity metric is calculated to find out the matching exponents between the current input TEE frame and the prior frames. The typical foreground and background intensities of prior images are therefore used to construct the corresponding energy function. Finally, the CMF approach, accelerated with a graphic processing unit (GPU), is employed to achieve the aortic valve contours in real time.
Results The evaluation study contained 30 sequences, with each containing 62–146 short-axis TEE frames. The results were compared with the manual segmentation (ground truth). The average symmetric contour distance (ASCD), dice metric (DM) and the reliability of the algorithm reached 0.85 ± 0.21 mm, 0.96 ± 0.01 and 0.90 ($d = 0.95$), respectively, and the computation time was 57.04 ± 8.98 ms per frame.
Conclusion The experiment results reveal that the proposed method can achieve accurate and real-time segmentation of aortic valve from TEE sequence of short-axis view.

Keywords Aortic valve · Transesophageal echocardiography sequence · Image segmentation · Probability estimation · Continuous max-flow

Introduction

The aortic valve is an important cardiac structure and plays a key role in circulatory system. Therefore, it can cause a serious problem if the aortic valve malfunctions like the occurring of aortic stenosis (AS). AS is highly prevalent, especially in elderly people, and the morbidity rate is likely to increase with population aging [1]. Among the untreated patients, approximately 50 % die in the first 2 years after symptoms appear [2]. A definitive therapy to cure severe AS is the valve replacement procedure. However, many patients do not undergo this surgical procedure due to their advanced age or significant comorbidities. Transcatheter aortic valve implantation is a less invasive procedure for such group of

J. Cai
Department of Cardiosurgery, Ruijin Hospital, Shanghai, China

X. Zhuang
School of Naval Architecture, Ocean and Civil Engineering, Shanghai Jiao Tong University, Shanghai, China

Y. Nie · Z. Luo · L. Gu (✉)
School of Biomedical Engineering, Shanghai Jiao Tong University, Shanghai, China
e-mail: gulixu@sjtu.edu.cn

patients, to replace a bioprosthetic valve without the need of sternotomy or cardiopulmonary bypass, which relies heavily on intraoperative image guidance [3].

The real-time 2D ultrasound (US), such as the transesophageal echocardiography (TEE) and transthoracic echocardiography (TTE), is commonly used to visualize the intraoperative aortic valve in TAVI [4,5], due to its ability to capture the fast moving structures [6]. Compared with TTE, TEE places the transducer inside the esophagus and can obtain images with better image quality [7].

To provide an accurate position for valve replacement, several works have addressed the importance of registering the intraoperative TEE sequence to a dynamic 3D aortic model derived from the preoperative computed tomography. In this registration, segmenting the aortic valve from the TEE sequence is one of the fundamental steps [8]. However, obtaining the accurate and real-time segmentation is challenging, due to the following degradation factors [9,10]:

1. Leaflet motion: the three leaflets of the aortic valve can have intense change of positions and shapes during the valve's opening and closing movement in a cardiac cycle.
2. Artifacts: the heavy calcification of the leaflets causes large shadowing artifacts, and it is difficult to detect the artifacts in advance to guarantee that they would not interfere with the postoperative processing.
3. Speckle noise: speckle noise, inherent to US images, is also one of the major difficulties in our segmentation task.
4. Acquisition on polar coordinates: the US images are collected in the polar coordinate system, which leads to a nonuniform intersampling space.

All the frames of a TEE sequence are not reasonably accessible for simple but prohibitively time-consuming manual segmentation method. Therefore, the automatic or semi-automatic algorithms become increasingly desirable. Although a number of works have been investigated on the methodologies of aortic valve segmentation, the methods applicable to segmenting it from TEE sequences are limited. Yet the literature on echocardiography segmentation of other tissues, especially for left ventricle, is rich. The left ventricle is also a dynamic structure, as it needs to receive blood from the left atrium and pump it to the aorta. Therefore, the research on left ventricle segmentation can be a good reference for the aortic valve segmentation task. Early works on the left ventricle were done to segment the single frame, while the recent research has taken the whole cardiac cycle into consideration.

Wolf et al. [7] applied a semi-automatic segmentation algorithm called the restricted optimal path exploring segmentation (ROPES) to TEE data. After searching candidate contour points fulfilling a multiscale edge criterion, they are connected to generate a closed contour by minimizing a cost function.

Chen et al. [11] solved a coupled minimization problem for the segmentation of cardiac US images in long-axis view by incorporating a prior shape and intensity profiles in the active contour framework. The prior information helped to estimate the balance between the image information and the shape priors. The algorithm was applied to two-chamber end diastolic cardiac US images to trace the epicardial borders.

Carneiro et al. [12] proposed a segmentation method for the left ventricle from US data using deep neural networks and efficient searching methods. Their algorithm increased robustness to imaging conditions absent in training data and simplified the complicated search process of pattern recognition with high accuracy. However, it requires a large set of training images.

The mitral valve is another important cardiac valve, yet there are few methods reported to obtain an accurate segmentation result. Schneider et al. [6] presented a graph-cut-based algorithm for the segmentation from 3D US images. They adopted the max-flow algorithm to solve the optimization problem [13]. A single user-specified point near the center of the valve was required, but it was the only manual input. The algorithm iterates until the metrics converge, which make it operator-independent. Illustrative results were demonstrated on the 3D US images with closed mitral valves.

Lang et al. [9] used a continuous max-flow (CMF) approach to extract the aortic valve of TEE images from both short-axis and long-axis views. This method constructs an energy function using the prior information coming from the previous three segmentation results in a cardiac cycle. However, these previous segmentation results only represent parts of the aortic valve variation, thus make the segmentation accuracy compromised. The authors evaluated the algorithm on a small set of 8 subjects (122 images), and the computation time was not reported.

In this work, we propose a real-time aortic valve segmentation method from intraoperative short-axis view TEE sequences. The method is based on an improved probability estimation algorithm and the graphic processing unit (GPU) [14] accelerated CMF scheme. It consists of two steps: firstly, we construct the probability estimation from the manual segmentation results of a small number of selected frames. This probability estimation is used as reference for the typical foreground and background intensities, regarded as the a prior information. In the second step, the prior information is incorporated into the construction of the energy function of the GPU accelerated CMF approach. By using this prior information, the new method becomes robust against the degradation factors of the aortic valve images, which is significant for clinical applications. The main contribution of this work includes the four aspects:

1. To address the difficulties caused by the aortic valve motion, five prior images that mostly represent the differ-

ent positions and shapes of the aortic valve are selected among a cardiac cycle by an expert.
2. The traditional computation of the composite probability estimation (CPE) and single probability estimation (SPE) has the limitation of sparsity in the constructed probability maps, due to the small number of samples from the chosen prior images. In this work, we propose a new formulation of the probability estimation using the Bayesian theorem and Parzen window estimation. In addition, radial average intensity, instead of single intensity, is used to optimize the probability estimation. As a result, the probability map is more robust for all frames to be segmented.
3. The GPU accelerated CMF approach reduces the computation load and provides real-time segmentation, which has great significance for medical image segmentation, especially for the intraoperative sequence segmentation.
4. The proposed segmentation method was applied to the image-guided TAVI procedure on animal studies and achieved accurate results of the aortic valve annulus from the intraoperative TEE sequences in real time.

Methods

Method overview

The aortic valve structure from the short-axis view of TEE is shown in Fig. 1. When the three leaflets close, they can divide the valve into several discontinuous segments, and when they open, the short-axis view becomes as a whole. Here, our segmentation task is to delineate the annulus of the structure, in which the edges inside the valve are ignored.

The workflow of the proposed method is shown in Fig. 2. It includes two major steps:

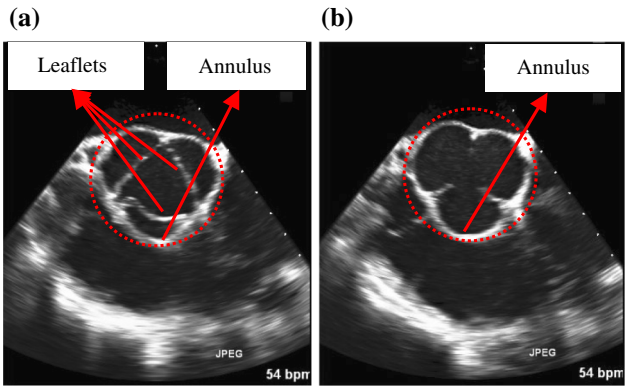

Fig. 1 Structure of aortic valve from short-axis view of TEE. **a** Closed aortic valve, **b** open aortic valve

1. Probability estimation stage: a new formulation of the probability estimation is proposed based on the Bayesian theorem and Parzen window estimation.
2. Energy function construction stage: appropriate energy functions are constructed for each frame to be segmentedle.

Continuous max-flow image segmentation

In continuous space, medical image segmentation with two regions can be described as a minimization problem of an energy function [15] (Eq. 1), which can be solved by the CMF approach [16]:

$$\begin{aligned}\arg\min_{\lambda\in[0,1]} E(\lambda) = &\int_{\Phi} (1-\lambda(x))\, C_s(x)\, \mathrm{d}x \\ &+ \int_{\Phi} \lambda(x)\, C_t(x)\, \mathrm{d}x \\ &+ \int_{\Phi} |\nabla\lambda(x)|\, C_p(x)\, \mathrm{d}x \end{aligned} \quad (1)$$

where Φ denotes the set of pixels in the image. $\lambda(x) \epsilon [0, 1]$ is a labeling function which labels image pixel x as foreground or background. $C_s(x)$ and $C_t(x)$ are regional properties that can be interpreted as penalties to assign a pixel as foreground or background based on image properties, respectively, and $C_p(x)$ is a boundary property, which represents a penalty for a discontinuity between two pixels. $|\nabla\lambda(x)|$ is the total variation of the labeling function.

Compared with the typical graph-cut approach on discrete space [13,17], CMF has an advantage of avoiding grid bias that can result in artifacts in the segmentation.

Probability estimation

Image gradients or differences in intensity distributions between the foreground and background are highly relied when segmenting ultrasound images [6,18,19]. However, because of the rapid motions and low image quality, it is difficult to utilize this information for obtaining accurate segmentation from TEE sequence.

As shown in Fig. 1, the shape of the annulus of the aortic valve resembles an ellipse, and the pixels close to the centroid of the manual segmentation have higher probability of being the foreground, regardless the intensity distributions. Therefore, to correctly delineate the annulus, a distance constraint should be considered. On the other hand, for the frame of a closed aortic valve, the pixels with high-intensity values near the centroid are corresponding to the three leaflets and more likely to be foreground, while the pixels with high-intensity values far from the centroid are corresponding to the edge of the aortic root and more likely to be background.

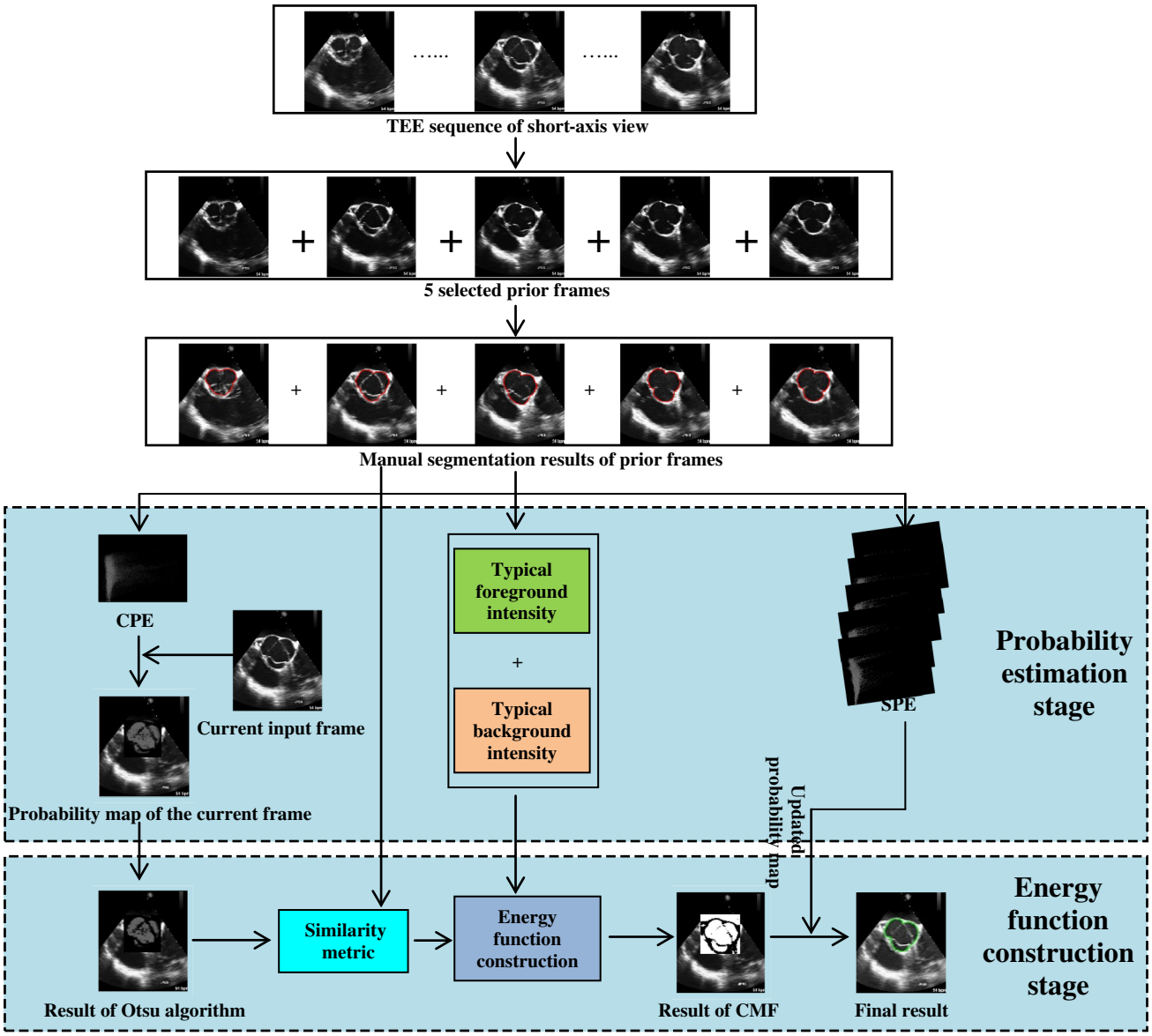

Fig. 2 Work flow of the proposed segmentation method

Therefore, intensity and radial distance can be both used to construct the probability estimation function, which was generated by calculating the conditional probability [4] of each pixel being the foreground based on its intensity and radial distance [9].

Radial average intensity In the previous work [20], single intensity of the current pixel was used with its radial distance to construct the CPE and SPE. However, when some segment of the aortic valve is blurry because of the rapid motion of the leaflets, it is very hard to accurately detect the valve contour. In order to tackle this problem, radial average intensity is applied to replace the single intensity of the current pixel to construct CPE and SPE, which makes full use of the adjacent pixels near the centroid in the radial direction, as shown in Eq. (2):

$$I^* = \frac{1}{n}\sum_{i=0}^{i=n} I_i \tag{2}$$

where I^* is the radial average intensity of the current pixel, I_0 is the single intensity of the current pixel, $I_i (i = 1, 2 \ldots n)$ represents the intensity of the n-th adjacent pixel near the centroid in the radial direction, and n is the number of the adjacent pixels (here, n is set to 5).

Formulation of probability estimation The traditional computation of the CPE and SPE has the limitation of sparsity in the constructed probability maps, due to the small number of samples from the chosen prior images [20]. A new formulation of the probability estimation is proposed here using the Bayesian theorem [21] and Parzen window estimation [22].

The probability map is defined to the posterior probability of the joint distribution, radial distance and intensity (R, I):

$$P\left(F|(R, I)\right) = \frac{P\left((R, I^*)|F\right) P(F)}{P\left(R,\ I^*\right)} \tag{3}$$

where $P(R,\ I^*)$ is the probability of a pixel whose radial distance and radial average intensity are R and I^*, respectively. $P(F)$ is the prior probability of being foreground, and the joint probability is estimated using the Parzen window method:

$$P\left(r, \iota|F\right) = \frac{1}{N_{\text{pz}}} \sum_{x\in\Omega} \omega_r\left(R(x)\right) \omega_\iota\left(I^*(x)\right) \tag{4}$$

where r and ι are, respectively, the discredited values of the radial distance and RAI, N_{pz} is the normalization term:

$$N_{\text{pz}} = \sum_{r\in R, \iota\in I^*} (r, \iota|F) \tag{5}$$

$\omega_r()$ and $\omega_\iota()$ are the Parzen window functions, which are the Gaussian kernel function in this work.

Computation of CPE and SPE Five different prior images, referred to as prior images {PI}, that can mostly represent the different positions and shapes of the aortic valve are selected from a cardiac cycle and manually segmented by an expert. The segmentation results are used as priors to estimate $P(F)$ and the joint distribution of (R, I^*).

For each segmentation result, a bounding box is calculated. Then, a maximum bounding box, covering the range of aortic valve movement in the TEE sequence, is determined using these five individual boxes. To ensure that the aortic valve is always covered, the maximum bounding box is further extended. In this study, x and y axes of the maximum bounding box are both extended by 20 %. In order to reduce the computational complexity, the TEE sequence segmentation is done within the extended maximum bounding box.

For SPE computation with one prior image, Eq. (3) can be used straightforwardly. The domain Ω in (4) is defined to the manually segmented foreground region in the corresponding prior image, and the radial distance of x, $R(x)$, is defined to its distance to the centroid of the domain Ω.

For CPE, the region Ω is defined to the concatenated volume of all the foreground regions in the prior images. The radial distance $R(x)$ is defined to its distance to the composite centroid. Therefore, for prior images PI_j, $j = 1 \ldots N_{\text{PI}}$, the computation of CPE is equivalent to:

$$P_{\text{CPE}}\left(F|(R, I)\right) = \frac{1}{N_{\text{PI}}} \sum_{j=1}^{j=N_{PI}} \frac{P\left((R, I^*)|F,\ PI_j\right) P(F|PI_j)}{P\left(R, I^*|PI_j\right)} \tag{6}$$

where N_{PI}, the number of prior images, is set to 5.

In addition, for each prior image PI_j, its typical foreground I_F^j and background intensities I_B^j, which can well represent the corresponding foreground and background intensities, are calculated, respectively, using Eqs. (7) and (8):

$$I_F^j = \sum_{x\in F} I(x) * P_{I(x)}^F \tag{7}$$

$$I_B^j = \sum_{x\in B} I(x) * P_{I(x)}^B \tag{8}$$

where F and B, respectively, denote the foreground region and the background region, P_I^F and P_I^B are, respectively, the probability of intensity I in foreground and background regions, and $I(x)$ is the intensity of pixel x. In this study, five groups of I_F^j and I_B^j are acquired.

Energy function construction

Similarity metric For the current input frame of the TEE sequence, the probability map is first obtained based on CPE, and then, Otsu algorithm is used to get an optimal threshold, where pixels with the intensity higher than the threshold are remained to comprise a target region A with a centroid C. Then, a similarity metric (SM) is applied to calculate the matching information between the prior images and the current input frame, as follows,

$$\text{SM}_j = \sum_{x\in A} \sqrt{\left(D_x - D_x^j\right)^2 + \left(I_x - I_x^j\right)^2} \tag{9}$$

where D_x is the distance from pixel x in A to C, and D_x^j is the distance from corresponding pixel x of prior image PI_j to its own centroid, I_x is the intensity of x, and I_x^j is the intensity of x in prior image PI_j. $D_x (D_x^j)$ and $I_x\ (I_x^j)$ are normalized by $D_{\max}$ and $I_{\max}$.

Lower SM means higher similarity, which contributes to find out the prior image best matching the current input frame of the TEE sequence, represented by P^* (with the lowest SM).

Energy function construction The probability map of current input frame is updated by the SPE of P^*. I_F and I_B of P^* are used to construct the energy function for the current input frame, as follows,

$$C_s(x) = |I_x - I_F| \tag{10}$$

$$C_t(x) = |I_x - I_B| \tag{11}$$

$$C_p(x) = 0.5 \tag{12}$$

where $C_s(x)$ and $C_t(x)$ are, respectively, the regional items representing the foreground and background, $C_p(x)$ is the boundary item.

Finally, a GPU accelerated CMF approach [16] is employed to get an initial segmentation result. The final result is obtained after the initial result is multiplied by the updated probability map.

Experiments and results

Experimental setting

The evaluation study contains 30 subjects (2,211 images), of which each has 62–146 short-axis TEE frames. The image data were acquired from a Philips iE33 ultrasound system with an X7-2t 3D TEE probe (Philips Health-care, Andover, MA). The experiments were performed under Windows XP on an Intel Core i7 computer with NVIDIA GeForce GTX 560 graphics card with 1 GB display memory and 256 bit data width. For evaluation purpose, the automatic segmentation results of the proposed method were compared with the corresponding manual segmentation, regarded as ground truth.

Scoring system

A scoring system, consisting of three error measures including average symmetric contour distance (ASCD), dice metric (DM) and reliability of the method, was employed to obtain quantitative performance assessment of the improved method. ASCD and DM are, respectively, based on contour and region, which are the most popular measures. They both measure the conformity between the ground truth and the automatic segmentation result.

Average symmetric contour distance (ASCD) ASCD is given in mm and based on the contour points of two segmentations A and M [23,24]. Here, A means the automatic segmentation result by the proposed algorithm, and M represents the ground truth. For an arbitrary contour point of A, $p(A)$, its Euclidean distance to the closest contour point of M is calculated using the approximate nearest neighbor technique [25] and stored, as shown in Eq. (13). To provide a symmetric measure, for arbitrary contour point of M, $p(M)$, its Euclidean distance to the closest contour point of A is also calculated using the same way, as shown in Eq. (14).

$$d\left(p\left(A\right), S\left(M\right)\right) = \min_{p(M)\in S(M)} \left\|p\left(A\right) - p(M)\right\| \tag{13}$$

$$d\left(p\left(M\right), S\left(A\right)\right) = \min_{p(A)\in S(A)} \left\|p\left(M\right) - p(A)\right\| \tag{14}$$

where $S\left(M\right)$ and $S\left(A\right)$, respectively, denote the set of contour points of M and A. ASCD is then defined as the average of all stored Euclidean Distance, as shown in Eq. (15):

$$\mathrm{ASCD} = \frac{1}{|S\left(A\right)| + |S\left(M\right)|} \left(\sum_{p(M)\in S(M)} d\left(p\left(M\right), S\left(A\right)\right) + \sum_{p(A)\in S(A)} d\left(p\left(A\right), S\left(M\right)\right) \right) \tag{15}$$

ASCD measures a distance between the ground truth and the automatic segmentation result. Therefore, lower ASCD means better conformity of the automatic segmentation result to the ground truth, and 0 represents an ideal segmentation result.

Dice metric (DM) DM measures the overlap between the regions surrounded by the automatic segmentation result and the ground truth [24], which is defined as:

$$DM = \frac{2R_{AM}}{R_A + R_M} \tag{16}$$

where R_A, R_M and R_{AM} are, respectively, the corresponding automatically segmented region, the corresponding manually segmented region, and the overlap between them. The region measurements are based on the number of pixels within each region.

As $R_{AM} \leqslant R_A(R_M)$, there is $0 \leqslant DM \leqslant 1$. Higher DM indicates better performance of the proposed method, and 1 means a perfect segmentation.

The reliability of the method The shape and position of the aortic valve can vary significantly across different cardiac phases of a scan, as well as across different scans. To measure the reliability of the method against this variation, we used the reliability metric, R(d), introduced in [24]:

$$\begin{aligned} R\left(d\right) &= P\left(DM > d\right) \\ &= \frac{\text{Number of frames with } DM > d}{\text{Total number of frames}} \end{aligned} \tag{17}$$

$R(d)$ indicates the reliability of the method with DM higher than $d(d \in [0, 1], 0 \leqslant R(d) \leqslant 1)$. The higher $R(d)$, the better the performance of the proposed method.

Evaluation of a representative sample

The study gives a representative sample for one subject over a whole cardiac cycle. For the subject, frames 1, 7, 10, 20 and 23 are choosed as prior images by an expert, and they are in the order of 0th, 1th, 2th, 3th and 4th. As shown in Fig. 3, the first row represents the manual segmentation results of the 5 prior frames, and the second row provides the corresponding SPEs. The 5 SPEs have two obvious common properties. First, from the x axis, since most of the target region of the valve has relatively low intensity (except the three leaflets which have relatively higher intensity), the SPEs are centralized in the area with low intensity, regardless of the distance.

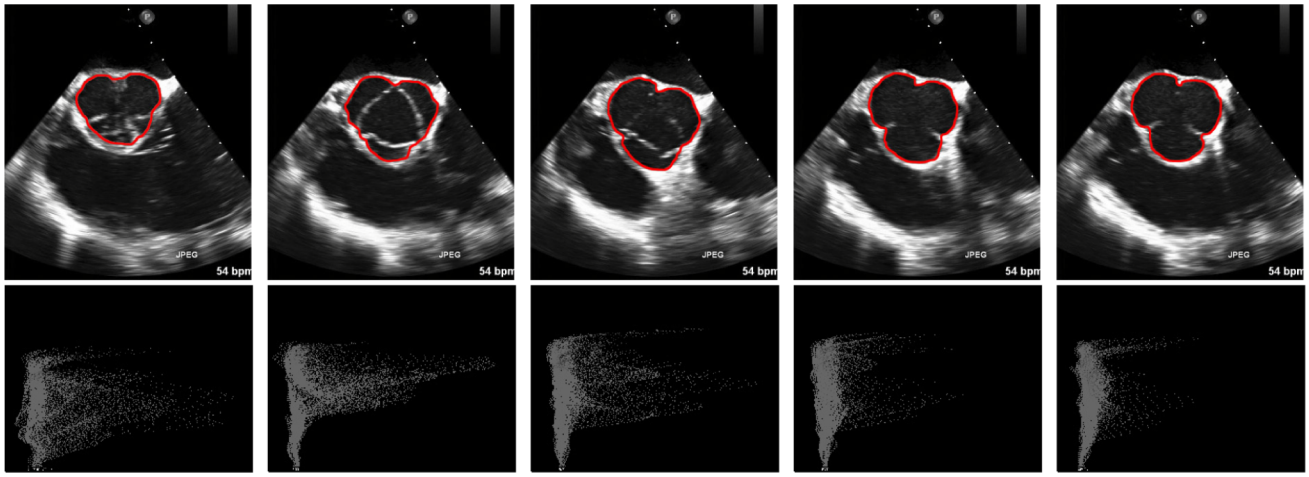

Fig. 3 Single probability estimation of prior frames, 1, 7, 10, 20, 23. The *first row* represents the five prior frames where *red curve* depicts the ground truth; the *second row* represents their corresponding single probability estimation, where the x axis represents radial average intensity and y axis represents the radial distance

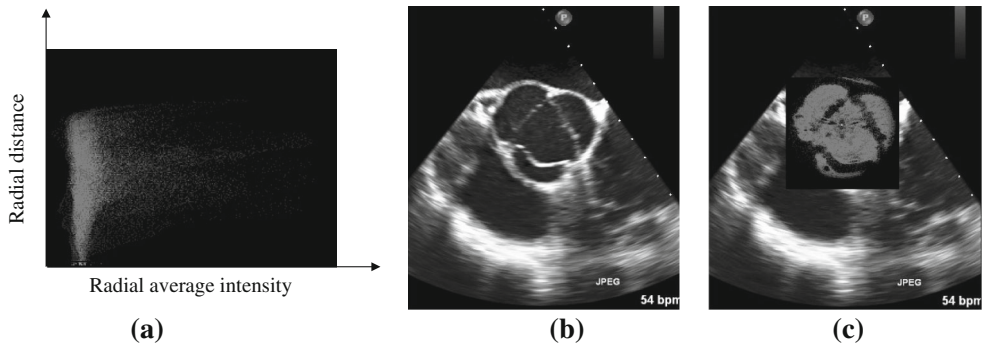

Fig. 4 **a** Composite probability estimation of prior frames; **b** the current input frame; **c** probability map of **b**

Second, from the y axis, the SPEs with small radial distance are very centralized while those with relatively large distance are scattered because of the leaflets. The SPEs with relatively high intensity and large distance represent the leaflets, and the others depict the other region of the valve. On the other hand, the aortic valve with different shapes and positions has different SPEs. Due to the motion of the leaflets, the SPE of closed valve is scattered in the area with relatively high intensity and large distance, while SPE of the open valve is centralized. In addition, the intervals of the intensity and distance are different for different prior frames. Figure 4a gives the CPE of prior frames, which has more uniform distribution than the SPEs. Figure 4b provides one current input frame, and Fig. 4c shows its corresponding probability map, where the rectangle around the valve is the dilated maximum bounding box.

The segmentation result of a representative sample is illustrated in Fig. 5. The green and red curves, respectively, represent the segmentation result of the proposed method and the ground truth. The example shows how the proposed method handles the large variations in the shape and position of the aortic valve and its computation time.

A TEE sequence over a whole cardiac cycle of this subject approximately contains 30 frames, which record the continuous and regular motion of the aortic valve. For frames 1–12 of the example subject, the aortic valve deformes from completely closed to gradually open. During this period, the three leaflets have big change in shape and position. For the rest 18 frames of the cardiac cycle, the aortic valve further deforms to completely open with slighter change of shape and position. Thus, Fig. 5 demonstrates typical segmentation results of 20 frames among a cardiac cycle, which indicates that the results of the proposed method have good correlation with the ground truth.

For frames 1–12, leaflet intensity is much higher than the other area of the foreground and is similar to the edge intensity. When the three leaflets are close to the centroid of the foreground, it is easy to obtain good segmentation result based on our method, like frame 36 and 37. But if they are very close to the edge, the leaflet can be potentially regarded

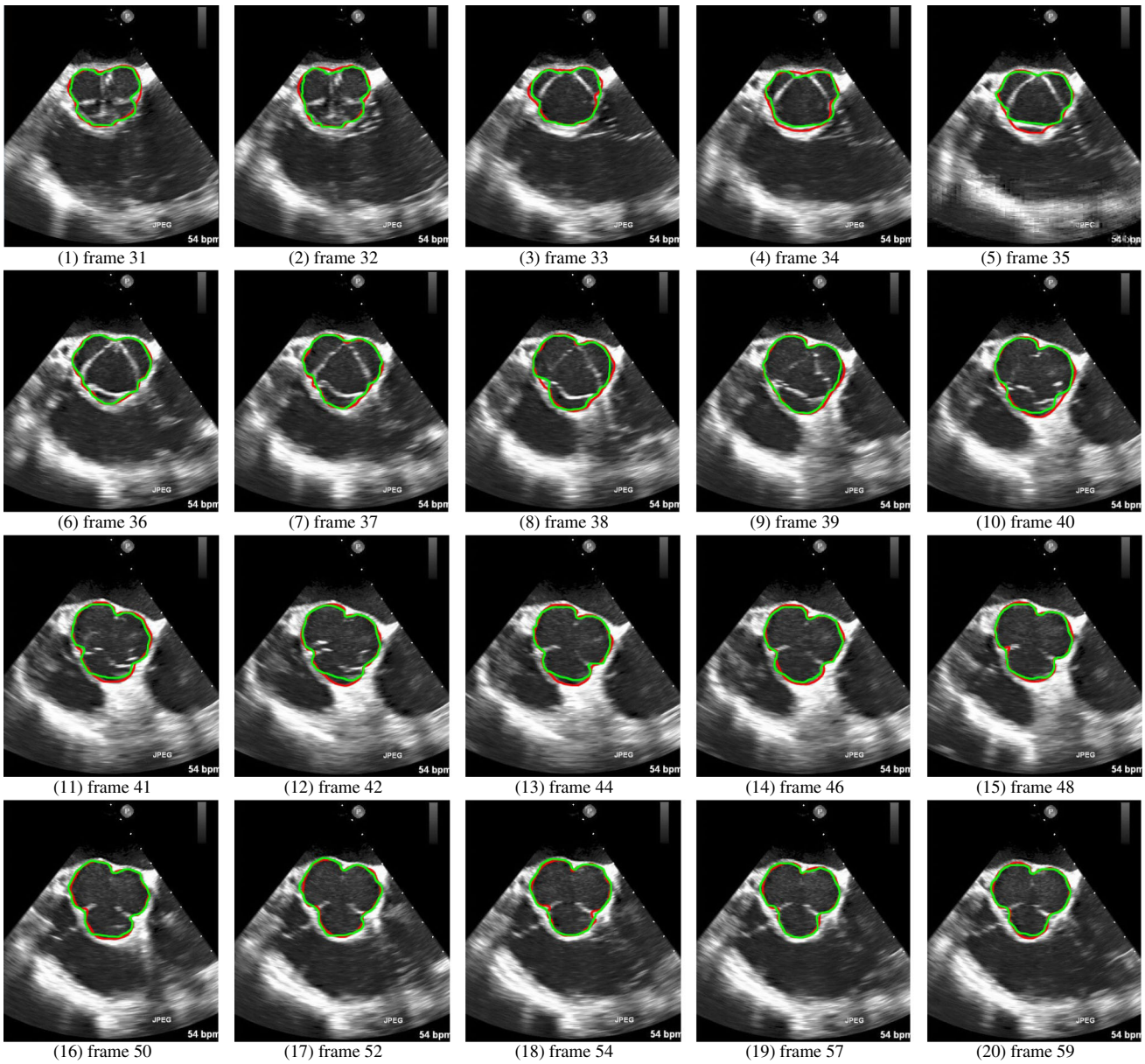

Fig. 5 Sequence segmentation results in a cardiac cycle for an example subject (*green curve* depicts the segmentation result of the proposed method; *red curve* represents the ground truth)

as background, like frame 35. For the rest 18 frames, the foreground and background of the aortic valve has big difference in intensity, which makes it easier to segment based on the proposed method.

Table 1 described the segmentation details about the example subject. Best match means the best matching one of the prior images for the current input frame based on similarity metric, which has the lowest SM. ASCD and DM measure the accuracy of the proposed method, and time (ms/frame) measures the computation time of the segmentation.

For the current input frame, it has the same best match with the previous frame or the next frame in most cases, which indicates the temporal and spatial continuity of the aortic valve. Among the 51st to the 60th frames, there are 9 frames that have the same best match (4th) due to the minor change of the aortic valve. The best match of frame 57 is different from the other 9 frames. Table 2 gives the similarity values between frame 57 and the prior frames. The third is the best matching one, and fourth is the second best matching one. The similarity metric between Frame 57 and the third is 0.0633772, and that between frame 57 and the fourth is 0.0650544, which are very close in fact. This confirms the temporal and spatial continuity of the aortic valve.

Table 1 Similarity metric of the sequence in a cardiac cycle for an example subject

Prior frames	Frame no.	Best match	Lowest SM	ASCD	DM	Time
	31	0th	0.0719856	0.966526	0.958027	65.32
	32	0th	0.1164920	1.152633	0.958860	55.17
	33	4th	0.1305630	1.111868	0.957618	73.28
	34	1th	0.1436000	1.048660	0.961014	46.12
	35	4th	0.1438800	1.315282	0.949242	64.01
	36	4th	0.1382050	1.244375	0.952393	74.02
	37	1th	0.0803825	0.610405	0.977744	50.69
	38	3th	0.0885252	1.024303	0.959161	45.76
	39	3th	0.1185420	0.638713	0.973847	51.45
	40	2th	0.0874847	0.738706	0.972669	52.33
	41	3th	0.1147660	0.895380	0.964423	67.81
	42	3th	0.1229320	1.018074	0.958092	54.73
1–0th	43	2th	0.1254650	0.796006	0.969007	50.65
7–1th	44	3th	0.1390120	0.643348	0.975309	68.97
10–2th	45	2th	0.1163350	0.728337	0.970380	41.46
	46	2th	0.1229620	0.706703	0.971994	46.11
20–3th	47	2th	0.1285550	0.703737	0.973190	55.78
23–4th	48	3th	0.1075520	0.671876	0.971704	52.84
	49	3th	0.0766738	0.673205	0.973524	61.46
	50	3th	0.0531003	0.617790	0.974763	45.69
	51	4th	0.0375209	0.674945	0.972719	64.98
	52	4th	0.0285839	0.677477	0.971694	65.05
	53	4th	0.0179098	0.997223	0.957942	50.55
	54	4th	0.0310928	0.768639	0.967497	51.63
	55	4th	0.0379531	1.001344	0.935344	62.22
	56	4th	0.0585121	0.829548	0.935525	49.46
	57	3th	0.0633772	0.537931	0.978623	60.67
	58	4th	0.0744649	0.727677	0.972238	51.06
	59	4th	0.0742130	1.138794	0.956821	66.73
	60	4th	0.0792282	0.775305	0.971952	65.34

Table 2 Similarity metric of frame 57

Prior frames	SM	Matching index
Frame 57		
0th	0.3008190	5
1th	0.1619790	3
2th	0.2297130	4
3th	0.0633772	1
4th	0.0650544	2

In order to intuitively evaluate the performance of the proposed method, Figs. 6 and 7 plot the ASCD and DM of the aortic valve segmentation as functions of time step. For most of the frames, the performance differs significantly over the cardiac cycle. Lower ASCD with higher DM means high similarity between the automatic segmentation result and the ground truth, indicating the automatic segmentation result has good correlation with the manual segmentation. Figure 8 plots the reliability of the proposed method as a function of $d(d = 0.93,\ R(d) = 1; d = 0.94,\ R(d) = 0.933;\ d = 0.95,\ R(d) = 0.9; d = 0.96,\ R(d) = 0.633;\ d = 0.97,\ R(d) = 0.5)$.

The overall performance of the proposed method over the 30 sequences and 2,211 frames is summarized in Table 3. Segmentation results of the proposed method correspond well with the ground truth, with ASCD and DM being 0.85 ± 0.21 mm and 0.96 ± 0.01, respectively. Based on the GPU accelerated CMF approach, the method achieved real-time segmentation for the TEE sequence. The computational

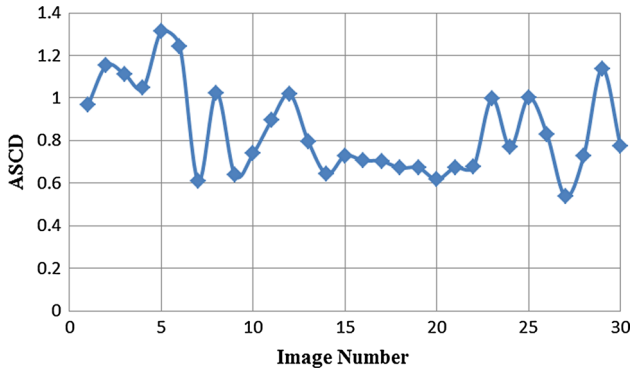

Fig. 6 Example of variation of ASCD as a function of the time step

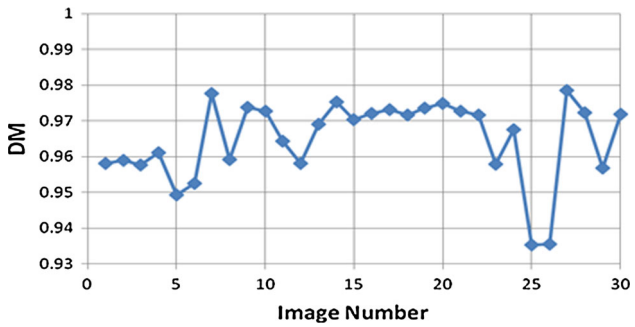

Fig. 7 Example of variation of DM as a function of the time step

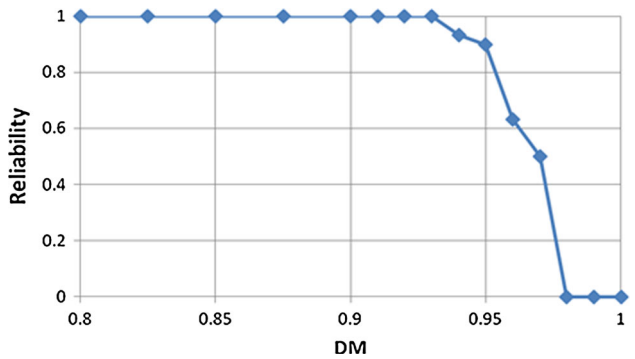

Fig. 8 Reliability of the proposed algorithm

Table 3 ASCD, DM, reliability of the algorithm and processing time per frame; ASCD and DM are expressed as mean ± SD

Items	ASCD	DM	Reliability ($d = 0.95$)	Time
Our method	0.85 ± 0.21	0.96 ± 0.01	0.90	57.04 ± 8.98

speed was increased by a factor of around 3.1 compared to that without GPU acceleration. As reported in Table 3, it only needs 57.04 ± 8.98 ms to segment a frame.

Discussions

To deal with challenges coming from the complex motions of the aortic valve, we combined the a prior information from multiple prior frames to assist the automated segmentation in TAVI, which improved the performance compared to the existing method [9]. This prior information is obtained offline, i.e., before the intervention procedure. During the intervention, the segmentation does not require any user interaction, meaning an automated and real-time delineation of the aortic valve throughout the whole intervention procedure.

The user selected five frames, which can best represent the different positions and shapes of the valve, as the prior frames from approximately 30 frames among a single cardiac cycle. Thus, they can further provide additional prior information for the segmentation. For each of the prior frames, both the SPE and the CPE were, respectively, constructed. The probability function is a joint distribution of the radial average intensity and the radial distance. The distance is relative to the centroid of the region of interest, which is defined in (3) and (6). Here, radial average intensity was used instead of single intensity of the current pixel. The adjacent pixels near the centroid in the radial direction were also taken into consideration. Radial average intensity made it easier to accurately detect the valve contour, especially for the blurry segments of the valve. To construct the CPE and SPEs, a new formulation, based on the Bayesian theorem and Parzen window estimation, was used to estimate the probability. Compared with the traditional computation in [20], this new method overcomes the limitation of sparsity in the constructed probability maps. For the sequence to be segmented, the GPU accelerated CMF approach significantly decreased the computation time, to only 1.7 s for the segmentation of a whole cardiac cycle. This computation time allows the aortic valve segmentation to be performed in real time.

To evaluate the proposed method, we compared our results with the manual segmentation, on a test dataset containing 30 sequences and 2,211 frames in total. It should be noted in Fig. 5 that our method have some slight deficiency in local concavities or convexities, but the overall segmentation result is accurate. The results demonstrated that the proposed method can reliably segment the aortic valve from the intraoperative TEE sequences, with ASCD and DM being 0.85 ± 0.21 mm and 0.96 ± 0.01, respectively. This can be considered a clinically acceptable performance. In addition, the reliability of the proposed method is 0.90 when $d = 0.95$, which illustrates good robustness when dealing with complex frames of the sequences.

Compared with [9], we not only combined the information from more prior TEE frames over a cardiac cycle, but also constructed both CPE and SPE. CPE is a probability function using all prior TEE frames, while SPE is a probability

function representing a specific prior TEE frame. Therefore, SPE contains prior probability distribution information of the prior frame best matching the current target frame. Finally, the probability function is a joint distribution of the radial average intensity and the distance relative to the geometric center of the region of interest, which is defined in (3) and (6).

For each input TEE frame, the typical foreground and background intensities of the best matching prior frame was used to construct the energy function of the current input TEE frame, making the construction more accurate. To get an impartial comparison, we selected the same number (i.e., three) of prior frames as [9]. The result reveals that the proposed method is superior (ASCD: 0.92 ± 0.23 mm versus 0.95 ± 0.88 mm [9]; DM: $95.5 \pm 1.2\,\%$ versus $94.0 \pm 2.0\,\%$ [9]).

The clinical realization of this approach could be feasible for image-guided TAVI procedure. TEE imaging itself is an attractive complement to CT and MRI during surgery, thanks to its safety, comparative low cost, ease of use, and being free from the compatibility problems between TEE imaging and standard OR equipments. Now, the proposed method solved the challenging problem of TEE segmentation in TAVI procedure by providing an accurate and real-time segmentation. It only needs to manually select and segment 5 prior frames before the procedure. Manual segmentation of the 5 prior frames can be obtained offline, and it has minimal disruption to the intraoperation. In the real-time scenario, the prior information becomes critical to maintain the high accuracy without decreasing computation efficiency, making the proposed method applicable in TAVI. We believe that our proposed method can make a good contribution to the image-guided TAVI procedure.

Conclusions

In this work, we have proposed a GPU accelerated CMF approach for aortic valve segmentation from intraoperative short-axis view TEE sequences using an improved probability estimation method. The strengths of this proposed method include: (1) selecting sequence-specific prior frames effectively, (2) constructing proper probability estimation, (3) providing accurate and real-time segmentation of the aortic valve. The segmentation method was validated on a large range of clinical data, and it achieved good performance. It should be noted that currently, the segmentation was validated on short-axis view frames of the aortic valve images, and these images were acquired from subjects suffering from slight or moderate AS. Therefore, our future work will focus on two aspects: (1) to improve the accuracy in dealing with local details based on active appearance models or object tracking and (2) to extend the segmentation to the long-axis view frames.

Acknowledgments This research is partially supported by the Chinese NSFC research fund (81301283, 61190120, 61190124, 61271318), SRF for ROCS, SEM, the Shanghai municipal health bureau research fund (2011216) and Biomedical engineering fund of Shanghai Jiao Tong University (YG2012MS21).

Conflict of interest Lixu Gu, Junfeng Cai, Xiahai Zhuang, Yuanyuan Nie and Zhe Luo declare that they have no conflict of interest.

References

1. Nkomo VT, Gardin JM, Skelton TN, Gottdiener JS, Scott CG, Enriquez-Sarano M (2006) Burden of valvular heart diseases: a population-based study. Lancet 368(9540):1005–1011
2. Leon MB, Smith CR, Mack M, Miller DC, Moses JW, Svensson LG, Tuzcu EM, Webb JG, Fontana GP, Makkar RR (2010) Transcatheter aortic-valve implantation for aortic stenosis in patients who cannot undergo surgery. N Engl J Med 363(17):1597–1607
3. Luo Z, Cai J, Gu L (2013) A pilot study on magnetic navigation for transcatheter aortic valve implantation using dynamic aortic model and US image guidance. Int J Comput Assist Radiol Surg 8(4):677–690
4. Masuda K, Kimura E, Tateishi N, Ishihara K (2001) Three dimensional motion mechanism of ultrasound probe and its application for tele-echography system. In: Proceedings. 2001 IEEE/RSJ international conference on intelligent robots and systems. IEEE, pp 1112–1116
5. Huber CH, Nasratulla M, Augstburger M, Von Segesser LK (2004) Ultrasound navigation through the heart for off-pump aortic valved stent implantation: new tools for new goals. J Endovasc Ther 11(4):503–510
6. Schneider RJ, Perrin DP, Vasilyev NV, Marx GR, del Nido PJ, Howe RD (2010) Mitral annulus segmentation from 3D ultrasound using graph cuts. IEEE Trans Med Imaging 29(9):1676–1687
7. Wolf I, Hastenteufel M, De Simone R, Vetter M, Glombitza G, Mottl-Link S, Vahl C-F, Meinzer H-P (2002) ROPES: A semiautomated segmentation method for accelerated analysis of three-dimensional echocardiographic data. IEEE Trans Med Imaging 21(9):1091–1104
8. Luo Z, Cai J, Peters TM, Gu L (2013) Intra-operative 2-D ultrasound and dynamic 3-D aortic model registration for magnetic navigation of transcatheter aortic valve implantation. IEEE Trans Med Imaging 32(11):2152–2165
9. Lang P, Rajchl M, McLeod AJ, Chu MW, Peters TM (2012) Feature identification for image-guided transcatheter aortic valve implantation. In: SPIE Medical Imaging. International Society for Optics and Photonics, pp 83162X–83162X-83114
10. Dias JM, Leitao JM (1996) Wall position and thickness estimation from sequences of echocardiographic images. IEEE Trans Med Imaging 15(1):25–38
11. Chen Y, Huang F, Tagare HD, Rao M (2007) A coupled minimization problem for medical image segmentation with priors. Int J Comput Vis 71(3):259–272
12. Carneiro G, Nascimento J, Freitas A (2010) Robust left ventricle segmentation from ultrasound data using deep neural networks and efficient search methods. In: 2010 IEEE international symposium on biomedical imaging: from nano to macro. IEEE, pp 1085–1088
13. Boykov Y, Kolmogorov V (2004) An experimental comparison of min-cut/max-flow algorithms for energy minimization in vision. IEEE Trans Pattern Anal Mach Intell 26(9):1124–1137
14. Rajchl M, Yuan J, Ukwatta E, Peters P (2012) Fast interactive multi-region cardiac segmentation with linearly ordered labels. In: 2012 9th IEEE international symposium on biomedical imaging (ISBI). IEEE, pp 1409–1412

15. Yuan J, Bae E, Tai X-C, Boykov Y (2010) A continuous max-flow approach to potts model. In: Daniilidis K, Maragos P, Paragios N (eds) Computer Vision-ECCV 2010. Springer, Berlin, pp 379–392
16. Yuan J, Bae E, Tai X-C (2010) A study on continuous max-flow and min-cut approaches. In: 2010 IEEE conference on computer vision and pattern recognition (CVPR). IEEE, pp 2217–2224
17. Boykov YY, Jolly M-P (2001) Interactive graph cuts for optimal boundary & region segmentation of objects in ND images. In: Proceedings. Eighth IEEE international conference on computer vision. ICCV 2001. IEEE, pp 105–112
18. Noble JA, Boukerroui D (2006) Ultrasound image segmentation: a survey. IEEE Trans Med Imaging 25(8):987–1010
19. Lang P, Rajchl M, Li F, Peters TM (2011) Towards model-enhanced real-time ultrasound guided cardiac interventions. In: 2011 International conference on intelligent computation and bio-medical instrumentation (ICBMI). IEEE, pp 89–92
20. Nie Y, Luo Z, Cai J, Gu L (2013) A novel aortic valve segmentation from ultrasound image using continuous max-flow approach. In: 2013 35th annual international conference of the IEEE engineering in medicine and biology society (EMBC). IEEE, pp 3311–3314
21. Hatt M, Cheze le Rest C (2009) A fuzzy locally adaptive Bayesian segmentation approach for volume determination in PET. IEEE Trans Med Imaging 28(6):881–893
22. Kwak N, Choi C-H (2002) Input feature selection by mutual information based on Parzen window. IEEE Trans Pattern Anal Mach Intell 24(12):1667–1671
23. Heimann T, Van Ginneken B, Styner MA, Arzhaeva Y, Aurich V, Bauer C, Beck A, Becker C, Beichel R, Bekes G (2009) Comparison and evaluation of methods for liver segmentation from CT datasets. IEEE Trans Med Imaging 28(8):1251–1265
24. Ben Ayed I, H-m Chen (2012) Max-flow segmentation of the left ventricle by recovering subject-specific distributions via a bound of the Bhattacharyya measure. Med Image Anal 16(1):87–100
25. Arya S, Mount DM, Netanyahu NS, Silverman R, Wu A (1994) An optimal algorithm for approximate nearest neighbor searching. In: Proceedings of the fifth annual ACM-SIAM symposium on Discrete algorithms. Society for Industrial and Applied Mathematics, Philadelphia, pp 573–582